Effect of Actuation Errors on a Purely-Translational Spatial Cable-Driven Parallel Robot

(Article begins on next page)

19 January 2025

Effect of Actuation Errors on a Purely-Translational Spatial Cable-Driven Parallel Robot

Giovanni Mottola[1], Clément Gosselin[2], *Fellow, IEEE*, and Marco Carricato[1], *Member, IEEE*

Abstract— In this paper, we analyze a spatial 3-DoF cable-driven robot with a finite-size end-effector. The robot has 6 cables that define 3 parallelograms, each composed by two cables: thus, the robot cannot rotate, but only perform translational motions. Also, since the two cables in a parallelogram are always kept at the same length, they can be actuated by the same motor, thereby meaning that the 3-DoF cable-suspended robot requires only 3 actuators. The kinematic and dynamic behaviour of such robots was studied in previous works. The property of purely-translational motion depends on a precise control of the extension of the cables. Therefore, in this paper we study how the platform pose changes as some errors of known maximum magnitude are introduced in the cable lengths. Finally, the results from both numerical simulations and tests are presented. The orientation of the platform is shown to be robust to cable extension errors.

I. INTRODUCTION

In cable-suspended parallel robots (CSPRs), the cables are kept in tension mainly by the weight of the end-effector (EE) and by inertia forces. They generally employ as many cables as the number of degrees of freedom (DoFs); such is the case of the robot considered here.

In industrial applications, one frequently needs to control the robot position, while the EE orientation has to remain constant. This can be achieved by a 6-cable robot, if cables are kept pairwise parallel and at the same length, so that they form 3 parallelograms. This allows a pair of cables to be controlled by a single actuator [1]–[6].

Since the property of translational motion relies on the special architecture and specific control actions, it is important to consider how errors in the control of cable lengths influence the platform pose. There is a vast literature [7] on *kinematic performance indices*, which are a way to measure the sensitivity of a robot to small control errors: here, we focus on *local* indices, which measure the sensitivity at a given pose (as opposed to *global* indices that average the sensitivity over the entire workspace). The *manipulability index* [8] and the *dexterity index* [9] are frequently used. However, the robotics community has not come to a consensus over the choice of such indices [10], [11], as they show some drawbacks.

Few studies are available on the sensitivity of CSPRs to control errors. The kinematic performance of a 3D printing CSPR with an architecture similar to the one considered

[1]G. Mottola and M. Carricato are with the Department of Industrial Engineering, University of Bologna, Italy giovanni.mottola3@unibo.it, marco.carricato@unibo.it
[2]C. Gosselin is with the Department of Mechanical Engineering, Université Laval, Québec, Canada gosselin@gmc.ulaval.ca
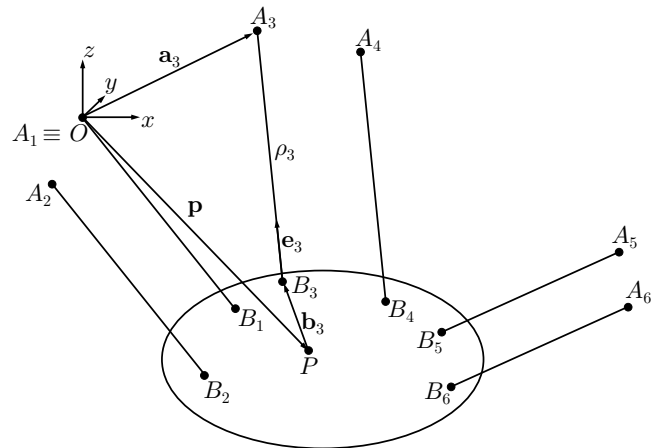
Fig. 1: A spatial, 6-cable CDPR with 3 translational DoFs.

here (but with six DoFs) was performed in [12], to verify that the maximum position error was within the printing accuracy; a kinematic index for a translational CDPR with a parallelogram-type actuation was also proposed in [4]. In this work, we analyze the kinematic performance of the translational CSPR with parallelogram-type actuation through kinematic indices inspired by [13] and [11], which overcome the shortcomings of other performance indicators.

Section II presents the static model of the robot. Sec. III introduces the new kinematic indices, discusses some of their properties, and applies them to study the effect of control errors in the translational CSPR. A practical architecture is then chosen and tested on a prototype (Sec. IV). Sec. V) concludes the paper by highlighting the advantages of the proposed architecture.

II. MODEL AND KINETOSTATIC ANALYSIS

A schematic drawing of the robot is presented in Fig. 1. The cable exit point A_i on the fixed frame has position vector $\mathbf{a}_i$ ($i = 1, ..., 6$) with respect to a fixed coordinate system $Oxyz$. The corresponding cable attachment point on the EE is B_i, while P is the EE centre of mass, with position vector $\mathbf{p} = P - O$. We also define the position vector $\mathbf{b}_i = B_i - P$: since the EE preserves its orientation, $\mathbf{b}_i$ is a constant vector. The cable length is $\rho_i = \|\mathbf{a}_i - \mathbf{p} - \mathbf{b}_i\|$ and the cable direction is $\mathbf{e}_i = (\mathbf{a}_i - \mathbf{p} - \mathbf{b}_i)/\rho_i$ (for obvious reasons, $\rho_i > 0$).

We assume that the motors are controlled so that, at every instant, $\rho_1 = \rho_2$, $\rho_3 = \rho_4$, and $\rho_5 = \rho_6$. We also require the fixed and mobile cable attachment points to be placed so that $\|\mathbf{a}_2 - \mathbf{a}_1\| = \|\mathbf{b}_2 - \mathbf{b}_1\|$, $\|\mathbf{a}_4 - \mathbf{a}_3\| = \|\mathbf{b}_4 - \mathbf{b}_3\|$, and $\|\mathbf{a}_6 - \mathbf{a}_5\| =$

$\|\mathbf{b}_6 - \mathbf{b}_5\|$, and that in the initial configuration cables $1-2$, $3-4$ and $5-6$ are pairwise parallel (so that $\mathbf{e}_1 = \mathbf{e}_2$, $\mathbf{e}_3 = \mathbf{e}_4$, and $\mathbf{e}_5 = \mathbf{e}_6$). In this way, the EE is suspended by three parallelograms: $A_1B_1B_2A_2$, $A_3B_3B_4A_4$, and $A_5B_5B_6A_6$. If all cables are taut, each parallelogram prevents the EE rotation about the direction $\mathbf{n}_{ij}$ normal to the plane Π_{ij} that contains the parallelogram. If the three vectors $\mathbf{n}_{ij}$ are not coplanar, all rotations are prevented, so the EE can only translate, and all parallelograms remain planar for finite motions [1], [6].

Cable i exerts on the EE a force $\mathbf{F}_i = \mathbf{e}_i\tau_i$ and a moment $\mathbf{M}_i = \mathbf{b}_i \times \mathbf{e}_i\tau_i$ with respect to P. When an external wrench $\mathbf{W}_e = [\mathbf{F}_e^T \ \mathbf{M}_e^T]^T$ acts on the EE, we can write the equilibrium equations for the robot as

$$\sum_{i=1}^{6} \mathbf{e}_i\tau_i = \mathbf{F}_e, \quad \sum_{i=1}^{6} \mathbf{b}_i \times \mathbf{e}_i\tau_i = \mathbf{M}_e \tag{1}$$

namely,

$$\mathbf{M}\boldsymbol{\tau} = \mathbf{W}_e \tag{2}$$

where $\boldsymbol{\tau} = [\tau_1, ..., \tau_6]^T$ and

$$\mathbf{M} = \begin{bmatrix} \mathbf{e}_1 & \mathbf{e}_1 & \cdots & \mathbf{e}_5 & \mathbf{e}_5 \\ \mathbf{b}_1 \times \mathbf{e}_1 & \mathbf{b}_2 \times \mathbf{e}_1 & \cdots & \mathbf{b}_5 \times \mathbf{e}_5 & \mathbf{b}_6 \times \mathbf{e}_5 \end{bmatrix} \tag{3}$$

In the definition of $\mathbf{M}$, we have used the property of cables being pairwise parallel. We thus have a linear system of six equations in six unknowns (the cable tensions τ_i). In [6], this system was simplified to form two decoupled systems (each of 3 equations in 3 unknowns). The first system to be solved is:

$$\mathbf{M}_{sup}\boldsymbol{\tau}_{tot} = \mathbf{F}_e, \ \mathbf{M}_{sup} = \begin{bmatrix} \mathbf{e}_1 & \mathbf{e}_3 & \mathbf{e}_5 \end{bmatrix} \tag{4}$$

where $\boldsymbol{\tau}_{tot} = [\tau_{tot,12}, \tau_{tot,34}, \tau_{tot,56}]^T$ is the vector of *total* cable tensions $\tau_{tot,ij} = \tau_i + \tau_j$. Each of the $\tau_{tot,ij}$'s is strictly greater than zero, otherwise at least one of the cables is not under tension; the conditions for positive $\tau_{tot,ij}$'s are described in [6].

The singularities of this robot are briefly recalled here [6]:

- an *actuation singularity* [14] occurs when $\mathbf{M}_{sup}$ is not invertible. This occurs when P lies on the plane Π defined by $A_{12}^* = \mathbf{a}_1 - \mathbf{b}_1 = \mathbf{a}_2 - \mathbf{b}_2$, $A_{34}^* = \mathbf{a}_3 - \mathbf{b}_3 = \mathbf{a}_4 - \mathbf{b}_4$, and $A_{56}^* = \mathbf{a}_5 - \mathbf{b}_5 = \mathbf{a}_6 - \mathbf{b}_6$.
- a *constraint singularity* [14] occurs when the matrix

$$\mathbf{A} = \begin{bmatrix} \mathbf{d}_{12} \times \mathbf{e}_1 & \mathbf{d}_{34} \times \mathbf{e}_3 & \mathbf{d}_{56} \times \mathbf{e}_5 \end{bmatrix} \text{diag}(\boldsymbol{\tau}_{tot}) \tag{5}$$

is singular (here, we have introduced $\mathbf{d}_{ij} = \mathbf{b}_i - \mathbf{b}_j$). In this case, vectors $\mathbf{n}_{ij}$'s are coplanar, so the robot is no longer purely translational, and gains a rotational DoF around the common normal to the $\mathbf{n}_{ij}$'s. The set of points such that $\det(\mathbf{A}) = 0$ corresponds to a quadric surface Σ.

In both singularities, the 6×6 matrix $\mathbf{M}$ in (2) is singular; the union of the singularity loci of $\mathbf{M}_{sup}$ and $\mathbf{A}$ provides the complete singularity locus of the manipulator.

A remarkable aspect of the translational robot studied here is that, unlike most parallel manipulators, its *direct Jacobian* $\mathbf{J} = \mathbf{M}^{-T}$ can be calculated analytically. First, let

$$\lambda_{e,ij} = \mathbf{e}_i \times \mathbf{e}_j, \ \boldsymbol{\pi}_i = \mathbf{e}_i \times \mathbf{b}_i, \ \boldsymbol{\pi}_{ij} = \boldsymbol{\pi}_i - \boldsymbol{\pi}_j \tag{6}$$

from which we get

$$\det(\mathbf{M}_{sup}) = \mathbf{e}_1 \times \mathbf{e}_3 \cdot \mathbf{e}_5 \tag{7a}$$
$$\det(\mathbf{A}) = -\tau_{tot,12}\tau_{tot,34}\tau_{tot,56}\pi_A \tag{7b}$$

where $\pi_A = \boldsymbol{\pi}_{12} \times \boldsymbol{\pi}_{34} \cdot \boldsymbol{\pi}_{56}$. Then, let

$$\mathbf{J}_{p,1} = + \lambda_{e,51}(\boldsymbol{\pi}_{56} \cdot \boldsymbol{\pi}_3 \times \boldsymbol{\pi}_4) + \lambda_{e,13}(\boldsymbol{\pi}_{34} \cdot \boldsymbol{\pi}_6 \times \boldsymbol{\pi}_5) \tag{8a}$$
$$\qquad + \lambda_{e,35}(\boldsymbol{\pi}_2 \cdot \boldsymbol{\pi}_{56} \times \boldsymbol{\pi}_{34})$$

$$\mathbf{J}_{p,2} = -\mathbf{J}_{p,1} - \lambda_{e,35}(\boldsymbol{\pi}_{12} \cdot \boldsymbol{\pi}_{56} \times \boldsymbol{\pi}_{34}) \tag{8b}$$

$$\mathbf{J}_{p,3} = + \lambda_{e,13}(\boldsymbol{\pi}_{12} \cdot \boldsymbol{\pi}_5 \times \boldsymbol{\pi}_6) + \lambda_{e,35}(\boldsymbol{\pi}_{56} \cdot \boldsymbol{\pi}_2 \times \boldsymbol{\pi}_1) \tag{8c}$$
$$\qquad + \lambda_{e,51}(\boldsymbol{\pi}_4 \cdot \boldsymbol{\pi}_{12} \times \boldsymbol{\pi}_{56})$$

$$\mathbf{J}_{p,4} = -\mathbf{J}_{p,3} - \lambda_{e,51}(\boldsymbol{\pi}_{34} \cdot \boldsymbol{\pi}_{12} \times \boldsymbol{\pi}_{56}) \tag{8d}$$

$$\mathbf{J}_{p,5} = + \lambda_{e,35}(\boldsymbol{\pi}_{34} \cdot \boldsymbol{\pi}_1 \times \boldsymbol{\pi}_2) + \lambda_{e,51}(\boldsymbol{\pi}_{12} \cdot \boldsymbol{\pi}_4 \times \boldsymbol{\pi}_3) \tag{8e}$$
$$\qquad + \lambda_{e,13}(\boldsymbol{\pi}_6 \cdot \boldsymbol{\pi}_{34} \times \boldsymbol{\pi}_{12})$$

$$\mathbf{J}_{p,6} = -\mathbf{J}_{p,5} - \lambda_{e,13}(\boldsymbol{\pi}_{56} \cdot \boldsymbol{\pi}_{34} \times \boldsymbol{\pi}_{12}) \tag{8f}$$

and

$$\mathbf{J}_{r,1} = \boldsymbol{\pi}_{56} \times \boldsymbol{\pi}_{34} \tag{9a}$$
$$\mathbf{J}_{r,3} = \boldsymbol{\pi}_{12} \times \boldsymbol{\pi}_{56} \tag{9b}$$
$$\mathbf{J}_{r,5} = \boldsymbol{\pi}_{34} \times \boldsymbol{\pi}_{12} \tag{9c}$$

Finally, one finds $\mathbf{J} = [\mathbf{J}_p^T \ \mathbf{J}_r^T]^T$, with

$$\mathbf{J}_p = \begin{bmatrix} \mathbf{J}_{p,1} & \mathbf{J}_{p,2} & \mathbf{J}_{p,3} & \mathbf{J}_{p,4} & \mathbf{J}_{p,5} & \mathbf{J}_{p,6} \end{bmatrix} \frac{1}{\det(\mathbf{M}_{sup})\pi_A} \tag{10a}$$

$$\mathbf{J}_r = \begin{bmatrix} \mathbf{J}_{r,1} & -\mathbf{J}_{r,1} & \mathbf{J}_{r,3} & -\mathbf{J}_{r,3} & \mathbf{J}_{r,5} & -\mathbf{J}_{r,5} \end{bmatrix} \frac{1}{\pi_A} \tag{10b}$$

III. KINEMATIC PERFORMANCE INDICES

The architecture proposed is based on specific assumptions on the robot architecture and on the way the robot is controlled, to guarantee that the motion is purely translational. Therefore, it is interesting to see how the robot behaves when we introduce the effect of errors in the control system, so that for example the two cables in a given pair $1-2$, $3-4$ or $5-6$ are not exactly at the same length: the cable pair, thus, no longer defines a parallelogram and small rotations are in fact possible. We then want to study the effect of errors $\pm\Delta\boldsymbol{\rho}$ in the actuators' commands (defined by the vector of cable lengths $\boldsymbol{\rho}$) at a given pose $\mathbf{p}$.

A. General properties

Both the manipulability [8] and the dexterity index [9] have a drawback that makes them unfit to study our translational architecture: they are based on the Jacobian, which in our case has non-homogeneous units. From the direct kinematics, $\mathbf{J}\dot{\boldsymbol{\rho}} = [\mathbf{v}^T \ \boldsymbol{\omega}^T]^T$, with $\mathbf{v}$ and $\boldsymbol{\omega}$ being the linear and angular velocity of the EE; thus, the first three rows of $\mathbf{J}$ have dimensionless entries, while the last three rows (corresponding to the rotational DoFs, which in our case are not actuated) have dimensions of the inverse of a length. The indices computed from $\mathbf{J}$ at a given pose[1] are then dependent

---

[1]Here, we use the ideal Jacobian, calculated at the reference pose as in (10). The implicit assumptions are that both actuator and pose displacements are measured with respect to the ideal pose and that the relationship between them can be linearized through a constant matrix.

on the measure units being used, while clearly the robot accuracy at a given pose is not.

Several authors have proposed different ways to overcome this issue. Some of the proposed methods are:

- to divide the rotational components of $\mathbf{J}$ by a *natural length* [15], whose definition is however arbitrary; it is thus difficult to compare different architectures;
- to analyze the velocity kinematics of the robot through the velocities of a set of points on the EE [16]; in this way, $\mathbf{J}$ has homogeneous dimensions, but there is no general criterion to pick up such points on the EE.

To overcome these issues, the authors of Ref. [11] propose to separate the translational and the rotational DoFs. Errors on the EE pose are defined by a displacement $d\mathbf{p}$ and a rotation vector $d\boldsymbol{\phi}$; the relationship between actuator errors $d\boldsymbol{\rho}$ and pose errors is $\mathbf{J}d\boldsymbol{\rho} = [d\mathbf{p}^T \ d\boldsymbol{\phi}^T]^T$. Two kinematic indices describing the sensitivity of the robot position and orientation to actuator errors were then defined as follows:

$$\sigma_{r,q} = \max_{\|d\boldsymbol{\rho}\|_q=1} \|d\boldsymbol{\phi}\|_q \tag{11a}$$

$$\sigma_{p,q} = \max_{\|d\boldsymbol{\rho}\|_q=1} \|d\mathbf{p}\|_q \tag{11b}$$

with $\|\bullet\|_q$ being the q-norm ($q \geq 1$) of ($\bullet$).
These kinematic indices have desirable characteristics:

- they have a well-defined meaning, that is, $\max\{\|d\mathbf{p}\|_q\} = \sigma_{p,q}\|d\boldsymbol{\rho}\|_q$ and $\max\{\|d\boldsymbol{\phi}\|_q\} = \sigma_{r,q}\|d\boldsymbol{\rho}\|_q$;
- each of them is consistent in terms of dimensional units;
- they can be used to compare different architectures;
- σ_r does not depend on the choice of P, but σ_p does, which again corresponds to physical intuition.

A physically sound choice for $\|d\boldsymbol{\rho}\|_q$ would be the infinity norm, as this corresponds to limiting the error on each actuator position to be comprised within ± 1[2]. In this case, the method proposed in [11] calculates sensitivities by solving three linear programming problems for each index, at every pose of the robot, so that the computation of a sensitivity map becomes impractically long. Moreover, the ∞-norm is less meaningful for rotational errors; for example, in (11a), it corresponds to the largest element (in absolute value) of $d\boldsymbol{\phi}$, whose significance does not appear obvious.

A possible solution may be using different norms for $d\boldsymbol{\rho}$ and for $d\mathbf{p}$ and $d\boldsymbol{\phi}$, borrowing an idea presented in [13].

Combining insights from previous works, kinematic performance indices are here defined as follows:

$$\sigma_{r,q,s} = \max_{\|d\boldsymbol{\rho}\|_q=1} \|d\boldsymbol{\phi}\|_s \tag{12a}$$

$$\sigma_{p,q,s} = \max_{\|d\boldsymbol{\rho}\|_q=1} \|d\mathbf{p}\|_s \tag{12b}$$

The indices in (12) are dimensionally consistent; moreover, by taking $s = 2$ and $q = \infty$, the errors in both the joint and Cartesian space are measured in the most "natural" way.

This definition of sensitivity indices is analogous to the one in [17] for planar parallel manipulators with rigid links.

To the best of the authors' knowledge, the application of the kinematic indices in (12) to spatial cable-driven robots with both rotational and translational DoFs is novel.

Writing the Jacobian as in Sec. II, one has $d\mathbf{p} = \mathbf{J}_p d\boldsymbol{\rho}$ and $d\boldsymbol{\phi} = \mathbf{J}_r d\boldsymbol{\rho}$. With this, the equations in (12) become equivalent to the definition of a matrix norm $\|\bullet\|_{q,s}$ *induced* by $\|\bullet\|_q$ and $\|\bullet\|_s$ [18], namely:

$$\sigma_{r,q,s} = \|\mathbf{J}_r\|_{q,s} \tag{13a}$$

$$\sigma_{p,q,s} = \|\mathbf{J}_p\|_{q,s} \tag{13b}$$

Calculating the kinematic sensitivities from matrix norms avoids having to solve the (generally nonlinear) convex optimization problem defined by (12). However, it was proven in [19] that even *approximating* (up to a given relative error) $\|\bullet\|_{\infty,s}$ is in general NP-hard, meaning that no known algorithm can do so in polynomial time; NP-hard problems become quickly intractable as the size of the input (in the case at hand, the size of matrices $\mathbf{J}_r$ and $\mathbf{J}_p$) grows. The maximum of $\|\mathbf{J}d\boldsymbol{\rho}\|_s$ for $\|d\boldsymbol{\rho}\|_\infty \leq 1$ must occur, for any $\mathbf{J}$, at a vector $d\boldsymbol{\rho}$ whose elements are either 1 or -1 (since the maximum over a polytope of a q-norm is attained at a vertex [20]). Therefore, it is necessary to evaluate $\|\mathbf{J}d\boldsymbol{\rho}\|_s$ in 2^{n_A} points (where n_A is the number of actuators); since usually in parallel robots $n_A \leq 6$, the computation times are in fact still reasonable[3].

It can be proven [21] from the general properties of matrix norms [18] that some of the interesting features of the indices defined in (11) still apply to the ones employed here. For instance, such indices provide upper bounds on the EE displacement and rotation under joint errors of known maximum absolute value $d\rho_{max}$, that is, $\|d\mathbf{p}\|_s \leq \sigma_{p,\infty,s}d\rho_{max}$ and $\|d\boldsymbol{\phi}\|_s \leq \sigma_{r,\infty,s}d\rho_{max}$. Moreover, these bounds are *tight*, meaning that there is at least one vector $d\boldsymbol{\rho}$ such that the corresponding error reaches its maximum value.

One might also be interested in comparing the proposed indices with the ones in previous works, for instance against the kinematic sensitivities from [11]. It can be proven that

$$\|\mathbf{J}\|_{\infty,2}/\sqrt{n} \leq \|\mathbf{J}\|_2 \leq \|\mathbf{J}\|_{\infty,2} \tag{14a}$$

$$\|\mathbf{J}\|_{\infty,2}/\sqrt{m} \leq \|\mathbf{J}\|_\infty \leq \|\mathbf{J}\|_{\infty,2} \tag{14b}$$

for any $m \times n$ matrix $\mathbf{J}$, including $\mathbf{J}_p$ and $\mathbf{J}_r$ [21]. Hence, considering a non-redundant parallel robot outside a singularity pose, the indices $\sigma_{p,2}$ and $\sigma_{p,\infty}$ from [11] can be computed with the matrix norms $\|\bullet\|_\infty$ and $\|\bullet\|_2$; this implies $\sigma_{p,\infty,2}/\sqrt{6} \leq \sigma_{p,2} \leq \sigma_{p,\infty,2}$ and $\sigma_{p,\infty,2}/\sqrt{3} \leq \sigma_{p,\infty} \leq \sigma_{p,\infty,2}$ (note that in this case the matrices $\mathbf{J}_p$ and $\mathbf{J}_r$ are 3×6). Similar inequalities can be written for the rotational sensitivity index. The proposed indices thus provide bounds for the ones already established in the literature.

B. Application to translational robot

When the robot approaches a constraint singularity, $\det(\mathbf{A}) \to 0$, so $\pi_A \to 0$; from (10), all entries of $\mathbf{J}_r$ and $\mathbf{J}_p$ go to infinity and so do σ_p and σ_r. If the robot approaches

---

[2]The maximum absolute error is set for convenience to be 1 in a suitable system of units; however, with the definitions used here, we are implicitly assuming that the errors are infinitesimal with respect to cable lengths.

[3]Note that $\|\mathbf{J}d\boldsymbol{\rho}\|_s = \|\mathbf{J}(-d\boldsymbol{\rho})\|_s$, so it is not necessary to check both $d\boldsymbol{\rho}$ and $-d\boldsymbol{\rho}$: the search space is thus halved.

an actuation singularity, instead, $\det(\mathbf{M}_{sup}) \to 0$, the entries of $\mathbf{J}_p$ go to infinity and $\sigma_p \to 0$, while σ_r remains finite.

In Fig. 2, we show the contour curves of σ_r and σ_p for an example architecture. As expected, the sensitivities become very high close to the singularity quadric Σ and to the singularity plane Π. In particular, both indices tend to infinity close to Σ; meanwhile, σ_p tends to infinity close to Π, while σ_r remains finite, so the rotational singularity (in Σ) and the translational one (in Π) are partially decoupled.

In [6], it was found that, if P is in the intersection of segments $\overline{B_1B_2}$, $\overline{B_3B_4}$ and $\overline{B_5B_6}$, the dynamic equations (1) can be greatly simplified. It can also be shown that for this architecture $\mathbf{J}_p$ is finite if and only if $\mathbf{M}_{sup}$ is invertible, so σ_p is finite everywhere except at a translational singularity: the two singularities are thus completely decoupled. A further specialization of this architecture is defined by P being on the midpoint of segments $\overline{B_iB_j}$: this choice also appears sensible from an engineering point of view, as it leads to having equal tensions in the two cables of each parallelogram [6]. Equations (10) simplify in this case as

$$\mathbf{J}_p = \frac{\mathbf{M}_{sup}^{-T}}{2} \begin{bmatrix} 1 & 1 & 0 & 0 & 0 & 0 \\ 0 & 0 & 1 & 1 & 0 & 0 \\ 0 & 0 & 0 & 0 & 1 & 1 \end{bmatrix} \tag{15a}$$

$$\mathbf{J}_r = \frac{\mathbf{A}'^{-T}}{2} \begin{bmatrix} 1 & -1 & 0 & 0 & 0 & 0 \\ 0 & 0 & 1 & -1 & 0 & 0 \\ 0 & 0 & 0 & 0 & 1 & -1 \end{bmatrix} \tag{15b}$$

with $\mathbf{A}'$ defined in the Appendix. The sensitivities can then be calculated as $\sigma_r = \|\mathbf{A}'^{-T}\|_{\infty,2}$ and $\sigma_p = \|\mathbf{M}_{sup}^{-T}\|_{\infty,2}$; this further reduces the computational cost, as the matrices involved have a smaller size.

Furthermore, in this case $\mathbf{J}_p$ (and thus σ_p) only depends on the EE position, but not on vectors $\mathbf{b}_i$: the positional sensitivity is thus independent of the size of the EE (as measured by the largest distance from the attachment points B_i to P). As for σ_r, it can be proven that, for a given size of the EE, it is minimized when the three segments $\overline{B_iB_j}$ are of equal length, in which case σ_r is inversely proportional to the EE size. This suggests that, in order to optimize the rotational sensitivity, and thus have a better chance of preventing rotations of the platform, we should place all B_i's at the same distance from P, and that this distance should be the largest compatible with size and weight constraints, which also corresponds to physical intuition.

These results and the ones from [6] suggest to design the EE with its attachment points B_i on a circle with centre on P, and to position all cable exit points A_i on a plane Π parallel to the circle through points B_i; in this way, the singularity surfaces degenerate to the plane Π. Also, as seen in [6], there is no risk of cable interference, unless the robot is in the singularity plane. This is the principle used in the design of our prototype (see Sec. IV). The final result is an architecture similar to the one in [5].

With this architecture, having points A_i's and B_i's on horizontal planes, it seems interesting to separate sensitivities along x and y axes, and along z. To do this, we further subdivide the matrices in $\mathbf{J}$ as $\mathbf{J}_p = \begin{bmatrix} \mathbf{J}_{p,xy}^T & \mathbf{J}_{p,z}^T \end{bmatrix}^T$ and
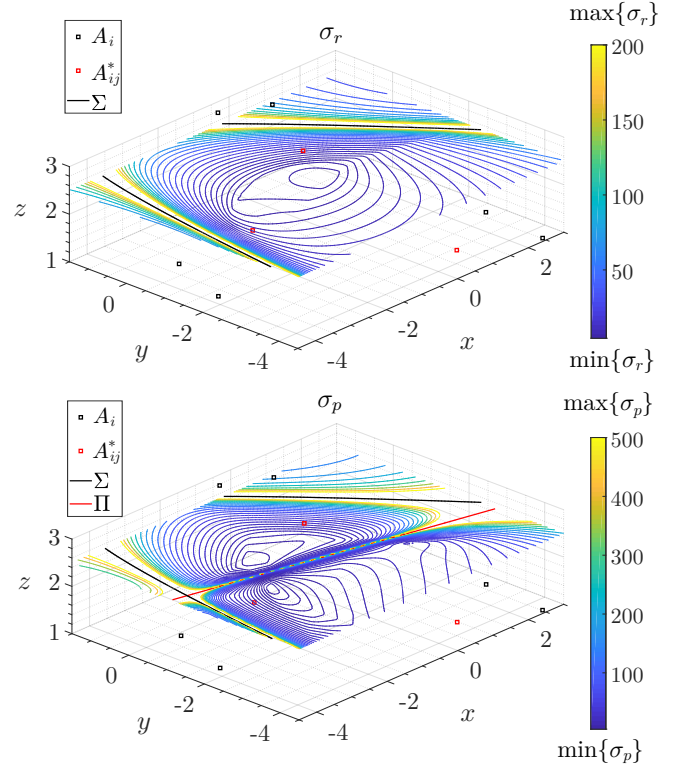

Fig. 2: The rotational (above) and translational (below) sensitivities calculated at a reference height z_r. The cable attachment points are represented as squares (the EE and the cables are not shown). Notice that σ_r and σ_p reach high values (in yellow, see colorbars) close to the singularity quadric Σ (whose intersection with the plane $z = z_r$ is indicated in black) and the singularity plane Π (whose intersection is in red). Length unit is arbitrary.

$\mathbf{J}_r = \begin{bmatrix} \mathbf{J}_{r,xy}^T & \mathbf{J}_{r,z}^T \end{bmatrix}^T$, with $\mathbf{J}_{p,xy}$ and $\mathbf{J}_{r,xy}$ being 2×6 matrices and $\mathbf{J}_{p,z}$, $\mathbf{J}_{r,z}$ being 6-element row vectors. Then, we can define four separate sensitivity indices as $\sigma_{r,xy} = \|\mathbf{J}_{r,xy}\|_{\infty,2}$, $\sigma_{p,xy} = \|\mathbf{J}_{p,xy}\|_{\infty,2}$, $\sigma_{r,z} = \|\mathbf{J}_{r,z}\|_{\infty,2}$ and $\sigma_{p,z} = \|\mathbf{J}_{p,z}\|_{\infty,2}$. These indices are related to σ_r and σ_p as follows:

$$\max\{\sigma_{r,xy}, \sigma_{r,z}\} \leq \sigma_r \leq \sqrt{\sigma_{r,xy}^2 + \sigma_{r,z}^2} \tag{16a}$$

$$\max\{\sigma_{p,xy}, \sigma_{p,z}\} \leq \sigma_p \leq \sqrt{\sigma_{p,xy}^2 + \sigma_{p,z}^2} \tag{16b}$$

The results, for the robot used in our tests, are shown in Fig. 3; here, the sensitivities are calculated as a function of z. The results can be thus explained:

- $z \to \infty$: $\sigma_{r,z}$ increases, as vectors $\mathbf{n}_{ij}$ (normal to the planes Π_{ij} through each parallelogram) become approximately horizontal and thus close to being linearly dependent: therefore, the ability of the robot to prevent rotations around the z axis is reduced. As the cables become almost vertical, a motion of the platform in the horizontal $x-y$ plane causes only a small change in the cable lengths: therefore, $\sigma_{p,xy}$ also increases.

- $z \to 0$: all planes Π_{ij}'s coincide with a single horizontal plane, so the rotation along the z axis is blocked, but the
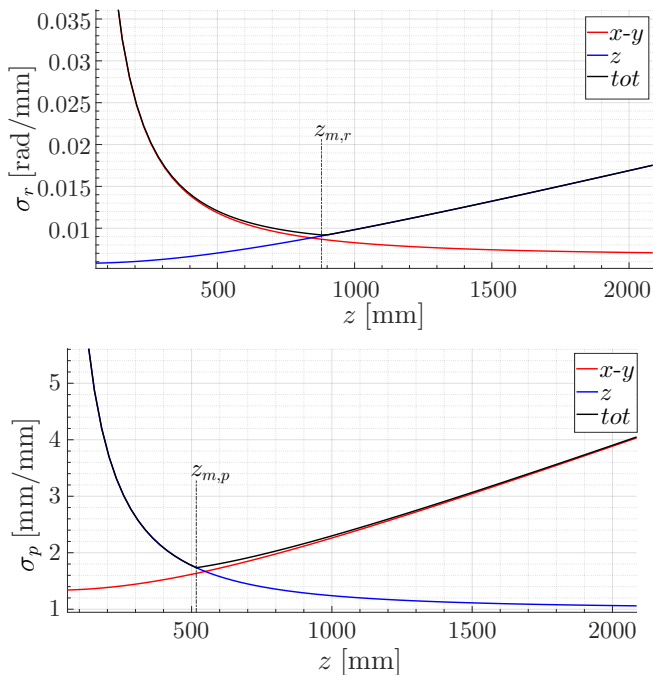
Fig. 3: The rotational (top) and translational (bottom) sensitivities calculated at $x = y = 0$ as functions of z, for the architecture used in the tests. Note that $\sigma_r, \sigma_p \to \infty$ as $z \to 0$ (close to the singularity) and for $z \to \infty$; σ_r and σ_p have a minimum respectively at $z = z_{m,r}$ and at $z = z_{m,p}$.
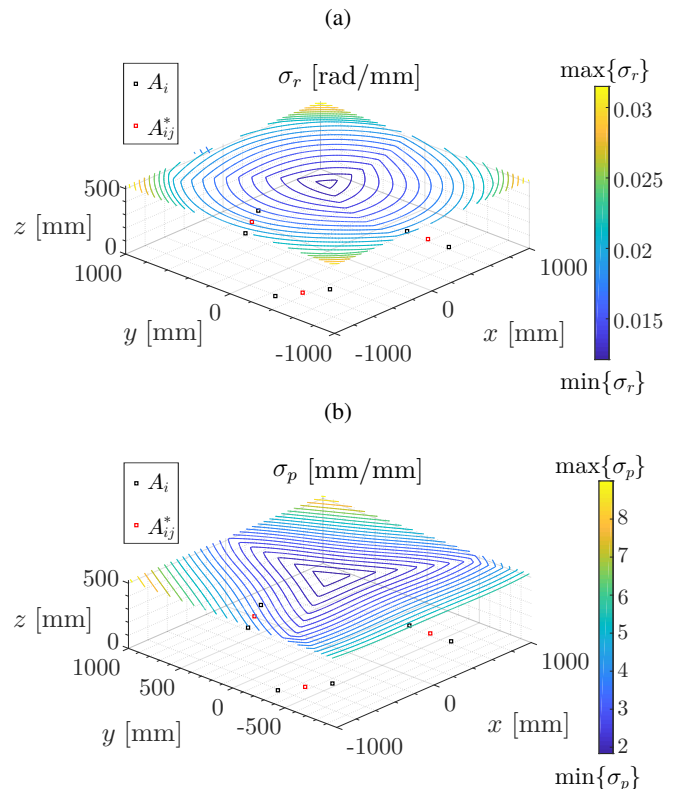
Fig. 4: The rotational (above) and translational (below) sensitivities for the prototype at a height $z_{m,p}$. The singularity surface $z = 0$ is not shown. The units of length are in mm.

EE can rotate along the x and y axes, thus $\sigma_{r,xy} \to \infty$. Also, we see that when P is on the singularity plane Π all cables are horizontal: the robot cannot move in plane Π, but it can have an infinitesimal motion in a direction normal to Π without changing the cable lengths. Therefore, $\sigma_{p,z}$ goes to infinity, too.

Fig. 3 suggests that there is an optimal interval of z where both indices σ_p and σ_r are generally smaller, between $z = z_{m,p}$ and $z = z_{m,r}$ (where respectively σ_p and σ_r are minimal). Therefore, an optimal height for the motion is between $z_{m,p}$ and $z_{m,r}$, depending on whether it is more important to have an accurate position or an accurate orientation. Given that, in the present case, σ_r does not change much around $z_{m,r}$, while the variation of σ_p in the neighborhood of $z_{m,p}$ is steeper, keeping $z \approx z_{m,p}$ during the motion appears as a sensible choice for an accurate horizontal positioning.

Figs. 4a and 4b show the plots of the sensitivity indices for the prototype. The indices are smaller towards the centre of the *static equilibrium workspace* (SEW, the set of points where the EE can be at rest with all cables taut): this indicates that the robot will be more accurate (both in terms of position and orientation) close to the centre, and less accurate close to the boundaries of the SEW (or even beyond said boundaries, using the dynamical trajectories from [6], [22]). This indicates that a trade-off must be considered when designing dynamic trajectories: these can enlarge the zone where the robot can work, but at the expense of a reduced accuracy. Note also the 120° symmetry of the plots in Figs.

4a and 4b, as expected due to the symmetry of the robot itself (where points A_{ij}^*'s are approximately on the vertexes of a equilateral triangle).

IV. EXPERIMENTAL TESTS

We performed tests on a CSPR prototype, with the same architecture (Fig. 5) as the one we used in [6]; the EE has the cable attachment points B_i at the same distance from P, as suggested by the analysis in Sec. III, to guarantee an acceptable rotational sensitivity in the entire SEW. Also, with this architecture cable interference and singularities are easily avoided, if the EE is below plane Π.

The results are shown in the video attached, where the robot is shown from two different viewpoints, one frontal and another above, as it performs some rest-to-rest motions. This trajectory is rather slow and does not take advantage of the dynamic properties of the robot, but rather serves to show its motion capability within the SEW. The robot clearly maintains a constant orientation and the cables remain parallel as the robot moves.

Finally, the sensitivity indices have been validated by comparing them against the errors observed during the tests. Fig. 6 shows the position error obtained by solving the *direct kinematic problem* (DKP) with both the target and the actual cable lengths (provided by the motor encoders) and calculating the distance $\|d\mathbf{p}\|_2$ between the target and actual position; the maximum error during motion was 6.93×10^{-3}
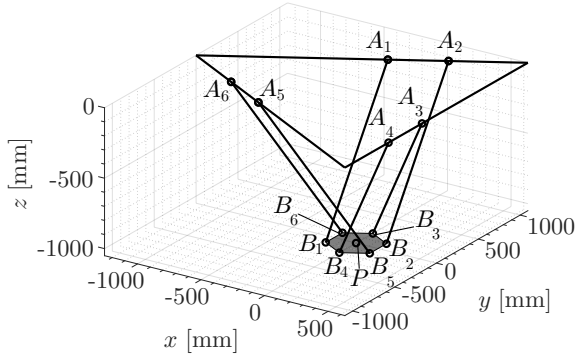
Fig. 5: A schematic of the robot in a reference pose, with $z \approx z_{m,r}$ (see Fig. 3). At this height, the rotational sensitivity is close to its minimum, so it is easier to prevent the robot from rotating. The fixed frame $Oxyz$ was chosen with its origin in the plane of points A_i, in the centre of the SEW.

m, which can be acceptable given the workspace size. Multiplying σ_p by the maximum error on the cable lengths $\|d\boldsymbol{\rho}\|_\infty$ (calculated at each time-step) provides an upper bound on the position error, as seen from the figure. This confirms that σ_p provides a useful upper bound to the error amplification between the joint and the Cartesian coordinates. Note that $\|d\mathbf{p}\|_2$ is obtained by solving a nonlinear DKP [1], while σ_p was defined assuming a linear relationship between $d\boldsymbol{\rho}$ and $d\mathbf{p}$: the correlation between the two plots in Fig. 6 suggests that this assumption (which is closer to the truth, the smaller the errors on the cable lengths are) is in fact valid.

V. CONCLUSIONS

In this paper, we considered a class of CSPRs with translational-only motion. We proved that the robot Jacobian can be written analytically, which is often not the case for parallel robots. From this, we found a computationally-efficient way of calculating the kinematic sensitivities for the rotational and the translational DoFs, and studied their behavior in proximity to a singularity condition.

We have also specialized the architecture defined in [6], which allows the dynamic equations for the robot to be simplified: for this particular architecture, we show how to place the mobile cable attachment points (for a given maximum size of the EE) in order to optimize the rotational sensitivity and, thus, to guarantee that orientation remains reasonably constant even in the presence of control errors.

Simulations and tests confirmed that the robot can move within its static workspace while keeping a stable orientation.

Future work includes the study of cable flexibility and its effect on the robot motion: here, for simplicity, cables were assumed to be massless and infinitely stiff.

APPENDIX

Here we analyze the special case introduced in Subsec. III-B. If P is on the midpoint of segments $\overline{B_i B_j}$, as in the special architecture introduced in Sec. III, it holds $\mathbf{b}_j = -\mathbf{b}_i$, so from (6) we have $\boldsymbol{\pi}_j = -\boldsymbol{\pi}_i$ and thus $\boldsymbol{\pi}_{ij} = 2\boldsymbol{\pi}_i$ and $\boldsymbol{\pi}_i \times$
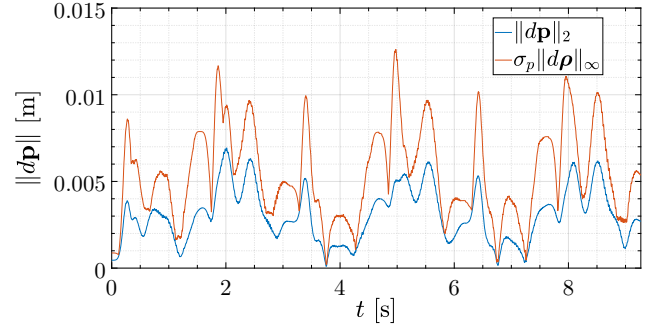

Fig. 6: Plot of the position error $\|d\mathbf{p}\|_2$ for the translational cable robot during the point-to-point motion (orange line) and the estimated maximum error (blue line) given by the position sensitivity, calculated along the same trajectory.

$\boldsymbol{\pi}_j = 0$ for each pair of cables i, j in the same parallelogram. Equations (8) and (9) simplify as

$$\mathbf{J}_{p,1} = -4\lambda_{e,35}(\boldsymbol{\pi}_1 \cdot \boldsymbol{\pi}_5 \times \boldsymbol{\pi}_3) = \mathbf{J}_{p,2} \qquad (17\text{a})$$

$$\mathbf{J}_{p,3} = -4\lambda_{e,51}(\boldsymbol{\pi}_3 \cdot \boldsymbol{\pi}_1 \times \boldsymbol{\pi}_5) = \mathbf{J}_{p,4} \qquad (17\text{b})$$

$$\mathbf{J}_{p,5} = -4\lambda_{e,13}(\boldsymbol{\pi}_5 \cdot \boldsymbol{\pi}_3 \times \boldsymbol{\pi}_1) = \mathbf{J}_{p,6} \qquad (17\text{c})$$

and

$$\mathbf{J}_{r,1} = 4\boldsymbol{\pi}_5 \times \boldsymbol{\pi}_3 \qquad (18\text{a})$$

$$\mathbf{J}_{r,3} = 4\boldsymbol{\pi}_1 \times \boldsymbol{\pi}_5 \qquad (18\text{b})$$

$$\mathbf{J}_{r,5} = 4\boldsymbol{\pi}_3 \times \boldsymbol{\pi}_1 \qquad (18\text{c})$$

Also, from (7), we obtain $\boldsymbol{\pi}_A = 8\boldsymbol{\pi}_1 \times \boldsymbol{\pi}_3 \cdot \boldsymbol{\pi}_5$. We also define matrix $\mathbf{A}' = [\boldsymbol{\pi}_1, \boldsymbol{\pi}_3, \boldsymbol{\pi}_5]$, from which we derive the rotational kinematic sensitivity seen in Subsec. III-B.

ACKNOWLEDGMENTS

REFERENCES

[1] P. Bosscher, R. Williams, and M. Tummino, "A concept for rapidly-deployable cable robot search and rescue systems," in *Proc. of the ASME 2005 IDETC/CIE*, Long Beach, USA, 2005, pp. 589–598.

[2] P. Bosscher, R. Williams *et al.*, "Cable-suspended robotic contour crafting system," *Automation in construction*, vol. 17, no. 1, pp. 45–55, 2007.

[3] A. Alikhani, S. Behzadipour *et al.*, "Workspace analysis of a three DOF cable-driven mechanism," *ASME J. Mech. Rob.*, vol. 1, no. 4, p. 041005, 2009.

[4] Z. Zhang, Z. Shao *et al.*, "Optimal design of a high-speed pick-and-place cable-driven parallel robot," in *Cable-Driven Parallel Robots*, C. Gosselin, P. Cardou *et al.*, Eds. Québec, Canada: Springer, 2018, pp. 340–352.

[5] D.-S. Vu, E. Barnett *et al.*, "On the design of a three-DOF cable-suspended parallel robot based on a parallelogram arrangement of the cables," in *Cable-Driven Parallel Robots*, C. Gosselin, P. Cardou *et al.*, Eds. Québec, Canada: Springer, 2018, pp. 319–330.

[6] G. Mottola, C. Gosselin, and M. Carricato, "Dynamically feasible motions of a class of purely-translational cable-suspended parallel robots," *Mech. Mach. Theory*, vol. 132, pp. 193–206, 2019.

[7] S. Patel and T. Sobh, "Manipulator performance measures-a comprehensive literature survey," *J. of Intelligent and Robotic Systems*, vol. 77, no. 3-4, pp. 547–570, 2015.

[8] T. Yoshikawa, "Analysis and control of robot manipulators with redundancy," in *Proc. of the 1st Int. Symp. Robotics Research*, Bretton Woods, USA, 1983, pp. 735–747.

[9] J. K. Salisbury and J. J. Craig, "Articulated hands: force control and kinematic issues," *Int. J. Rob. Res.*, vol. 1, no. 4, p. 417, 1982.

[10] J.-P. Merlet, "Jacobian, manipulability, condition number, and accuracy of parallel robots," *ASME J. Mech. Rob.*, vol. 128, no. 1, pp. 199–206, 2006.

[11] P. Cardou, S. Bouchard, and C. Gosselin, "Kinematic-sensitivity indices for dimensionally nonhomogeneous Jacobian matrices," *IEEE Trans. Robot.*, vol. 26, no. 1, pp. 166–173, 2010.

[12] E. Barnett and C. Gosselin, "Large-scale 3D printing with a cable-suspended robot," *Additive Manufacturing*, vol. 7, pp. 27–44, 2015.

[13] K. C. Olds, "Global indices for kinematic and force transmission performance in parallel robots," *IEEE Trans. Robot.*, vol. 31, no. 2, pp. 494–500, 2015.

[14] M. Conconi and M. Carricato, "A new assessment of singularities of parallel kinematic chains," *IEEE Trans. Robot.*, vol. 25, no. 4, pp. 757–770, 2009.

[15] J. Angeles, "The design of isotropic manipulator architectures in the presence of redundancies," *Int. J. Rob. Res.*, vol. 11, no. 3, pp. 196–201, 1992.

[16] C. Gosselin, "The optimum design of robotic manipulators using dexterity indices," *Robotics and Autonomous Systems*, vol. 9, no. 4, pp. 213–226, 1992.

[17] M. H. Saadatzi, M. T. Masouleh *et al.*, "Geometric analysis of the kinematic sensitivity of planar parallel mechanisms," *Trans. of the Canadian Soc. for Mechanical Eng.*, vol. 35, no. 4, pp. 477–490, 2011.

[18] D. S. Bernstein, *Matrix mathematics: theory, facts, and formulas*. Princeton University Press, 2009.

[19] J. M. Hendrickx and A. Olshevsky, "Matrix p-norms are NP-hard to approximate if $p \neq 1, 2, \infty$," *SIAM J. Matrix Anal. & Appl.*, vol. 31, no. 5, pp. 2802–2812, 2010.

[20] H. L. Bodlaender, P. Gritzmann *et al.*, "Computational complexity of norm-maximization," *Combinatorica*, vol. 10, no. 2, pp. 203–225, 1990.

[21] G. Mottola, "Dynamically feasible trajectories of fully-constrained cable-suspended parallel robots," Ph.D. dissertation, Alma Mater Studiorum - University of Bologna, 2019.

[22] G. Mottola, C. Gosselin, and M. Carricato, "Dynamically feasible periodic trajectories for generic spatial three-degree-of-freedom cable-suspended parallel robots," *ASME J. Mech. Rob.*, vol. 10, no. 3, p. 031004, 2018.